Globally Optimized Linear Windowed Tone-Mapping

Qi Shan, *Student Member, IEEE,* Jiaya Jia, *Member, IEEE,* and Michael S. Brown, *Member, IEEE*

Abstract—This paper introduces a new tone-mapping operator that performs local linear adjustments on small overlapping windows over the entire input image. While each window applies a local linear adjustment that preserves the monotonicity of the radiance values, the problem is implicitly cast as one of global optimization that satisfies the local constraints defined on each of the overlapping windows. Local constraints take the form of a guidance map that can be used to effectively suppress local high contrast while preserving details. Using this method, image structures can be preserved even in challenging high dynamic range (HDR) images that contain either abrupt radiance change, or relatively smooth but salient transitions. Another benefit of our formulation is that it can be used to synthesize HDR images from low dynamic range (LDR) images.

Index Terms—High dynamic range image, tone mapping, display algorithms, image enhancement, filtering.

1 Introduction

High dynamic range compression – or tone mapping – embodies techniques that map HDR images to low dynamic range displays that only have moderate contrast. While a global linear scaling can be used to compress the dynamic range, e.g. from 10000:1 to 200:1, the result will be undesirable since image structures are linearly flattened, causing the loss of the visual information mostly in highlights and shadows. To avoid this trivial solution, most tone mapping techniques employ some type of non-linear mapping functions. Several tone mapping algorithms have been proposed that either adjust the global tone response curve [14] or locally reproduce tonal values [7] [9] [16]. It is also generally noticed [9] [16] that local operators, which reproduce the tonal values in a spatially variant manner, perform more satisfactorily than global operators in terms of detail preservation and compression ratio of the dynamic range.

The objective in this paper is to develop a new tone reproduction operator. We observe that HDR in an image can typically be categorized into two types – 1) regions exhibiting significant high dynamic range but with smooth radiance transition (Figures 1(a)) and 2) regions exhibiting sharp and significant local radiance change among neighboring pixels (Figure 1(b)). Our tone reproduction operator provides a unified framework to effectively address these two types of HDR. Our approach maintains *local structures*, including sharp edges and smooth color transitions at a perceptual level while not introducing visible artifacts such as halos.

Fig. 1. HDR regions exhibiting abrupt and significant radiance change (upper right) and smoother local transition (lower right).

Our approach uses a window-based tone mapping method in which a *global* optimization problem is solved that satisfies *local* constraints. Specifically, our method operates on windows; in each window a linear function is used to constrain the tone reproduction in order to naturally suppress strong edges while retaining weak ones. The high dynamic range is compressed by solving an image-level optimization problem that integrates all window-based constraints.

While our method is regarded as a local operator, it does not involve scale decomposition, layer separation, or image segmentation, and is therefore less susceptible from the associated artifacts known with these previous procedures. Within our global optimization framework, the overall tone mapping effect is non-linear and spatially variant, and adapts to rich and diverse structures of images. Our method can be expressed with a closed-form solution that reaches a global optimum. Owing to the global optimality, any sufficient local tone adjustment in our method gives rise to a global effect where errors are minimized and distributed across the entire

- *Q. Shan and J. Jia are with the Department of Computer Science and Engineering, the Chinese University of Hong Kong, Hong Kong.*
  E-mail: {qshan, leojia}@cse.cuhk.edu.hk
- *M. S. Brown is with the Department of Computer Science, National University of Singapore.*
  E-mail: brown@comp.nus.edu.sg

image. Moreover, our method provides flexibility for image quality adjustments with only a few parameters, adaptive to various user requirements pertaining to the range compression ratio and the detail preserving ratio.

In addition to high dynamic range compression, our method also contributes a unified framework for tone enhancement of ordinary images by solving the same optimization problem. An application of synthesizing an HDR image from a single low dynamic range (LDR) image is presented to simulate the high contrast environment in indoor and outdoor scenes containing shiny light sources or obscure shadows. The effectiveness of our HDR synthesis is evaluated by comparisons against ground truth images.

The rest of our paper is organized as follows. Section 2 reviews related work. Section 3 presents our algorithm of HDR compression. Section 4 describes the parameter setting and shows our HDR compression results. Our algorithm is applied to ordinary image enhancement and HDR image synthesis as described in Section 5. Section 6 discusses the proposed approach and summarizes our work.

2 Previous Work

Tone mapping operators have attracted broad interests recently. Surveys of these methods can be found in [5] [25] [21]. We review HDR compression methods in two categories: global operators and local operators. The global tone mapping operators map the radiance values in a spatially invariant manner. Histogram based and sigmoid transfer function based algorithms, such as gamma correction, are two main categories of global operators. For global operators, the key problem is to establish a one-to-one or onto mapping from high dynamic radiance values to the low dynamic ones. Sigmoidal compression is to redistribute radiance values in an HDR image using a sigmoid curve. This results in low compression at the low and high end of the radiance range, with more compression in the mid-range. Sigmoid compression is a reasonable way to compress many HDR images. Other similar global functions with similar properties are discussed in detail in Chapters 6 and 7 of [21]. In [14] [6], non-linear global operators were proposed where global tone reproduction curves with different measures of image qualities are estimated to reduce the dynamic range in a computationally efficient way. These methods do not need manual tuning and are capable of producing visually satisfactory results for a large set of examples. However, these approaches may fail for HDR images where strong local contrast is present (i.e. a local region contains both high and low radiance values). Further, finding a perfect tone reproduction curve is difficult [4] for several cases.

Inspired by how the human visual system adapts to local regions of scene luminance [21], more sophisticated local tone reproduction methods have been proposed. Many of these approaches involve decomposing, compressing, and recombining layers in the HDR images. Krawczyk *et al.* [13] first segmented an HDR image, and then applied different tone reproduction curves to the segments to achieve spatially variant HDR compression. With appropriate algorithm design and implementation, no seams will be present in the tone mapping results.

In [24], an image is decomposed into a reflectance image R and an illuminance image L, according to the observation that the high dynamic range is generally caused by the illuminance, while reflectance is unlikely to produce high contrast. However, accurately separating the two layers from a single image is non trivial. To simplify the intrinsic image decomposition, it is assumed that L contains low frequency information while R may have spatially abrupt change in values [11]. Assuming the surface reflectance and illumination properties are known, Tumblin *et al.* [25] compressed high dynamic range only in the illuminance image. In [7], an image is decomposed into a base layer and a detail layer. The base layer is obtained using a bilateral filter, and the detail layer is computed by subtracting the base layer from the input image. A linear scaling in the logarithm domain of the base layer is performed to compress the dynamic range and the final result is the combined detail layer and the compressed base layer.

Other scale decomposition based techniques decompose the HDR images into several layers [12] [19] [26], imitating human vision adaptation to local changes. In [16], a multiscale approach using symmetrical analysis-synthesis filter banks and automatic gain control was proposed to compress the HDR images in subbands. This method, along with those in [20] [2], incorporated schemes to avoid so haloing artifacts. This type of artifacts, as explained in [16], can be considered as signal distortions that occurs when combining multiple compressed subband layers. It can often be reduced with careful selection of the parameter values.

Recently, in [8], a new edge-preserving multi-scale image decomposition method was proposed. Results demonstrate that this image decomposition method outperforms bilateral filtering in producing range compressed images.

Gradient domain dynamic range compression [9] does not directly process the image radiance. Instead, the tone mapping operator attenuates the image gradients with large magnitude while magnifying the small ones. The final result is computed by solving a Poisson equation. Lischinski *et al.* [17] presented an interactive method to locally adjust the tonal values and other visual parameters. In their method, the user uses a set of brushes to impose constraints on the image. Influence functions are computed to confine the modifications of the tonal value in image space.

Different from these methods, our local operator does not require multiscale decomposition or segmentation of the images into binary or fractional maps. This avoids problems associated with layer decomposition, including the decomposition itself as well as layer recombination. We directly process the radiance map where a *global op-*

timization framework is adopted to naturally constrain the respective pixel values in a global sense. In addition, our approach does not require any smoothness constraints to be imposed on the final output.

Inferring an HDR image from an LDR images is known as "inverse tone mapping" [3]. Single image methods can only achieve an approximation of the solution due to the information loss. In [3], high luminance areas are estimated from an LDR image. An inverse tone mapping operator, which reverses the technique in [20] is then applied to enhance luminance in the detected areas. Meylan *et al.* [18] proposed detecting the specular highlights in the LDR images and boosting the intensity in these regions. The LDR images generated in the tone mapping stage produce small errors in the dynamic range expansion stage. In [1], psychophysical studies showed that linear contrast scaling works well in most cases for expanding the dynamic range of some ordinary images. Rempel *et al.* [22] proposed a real-time technique to synthesize an HDR images by enhancing the brightness gradation in the saturated regions. In [16], Li *et al.* addressed a special HDR compression-expansion problem (a process called "companding", for example, to turn a 12 bit/channel image into an 8 bit/channel TIFF, and later convert it back to a good approximation of the original 12-bit image) by adopting a feedback-loop scheme. This method reconstructs an HDR image from an LDR image that was first tone-mapped with their subband technique. This approach, however, cannot be used to expand the dynamic range of an arbitrary LDR image.

Comparing our work with previous inverse tone mapping methods, our algorithm not only attempts to make the results look natural by enhancing pixel intensity more significantly in highlights, but also aims to produce results with radiance similar to that of the ground truth HDR images. Synthesizing an HDR image in our system can be regarded as a partial inverse of HDR compression. It is naturally solved in our unified framework without requiring large modifications of the system.

3 Algorithm and Implementation

Given an input HDR image with radiance map I^h, the high dynamic range compression operator $f(\cdot)$ computes the radiance map in a low dynamic range $I^l = f(I^h)$. An intuitive approach to designing a tone mapping operator is to decrease the large radiance values and increase small ones. To correctly retain the local structures, however, the monotonic mapping of radiance should be satisfied regarding each pixel's neighborhood in a small local region, similar to the monotone characteristic of the global tone mapping curves. Therefore, if we zoom into the square window w_i containing only a few pixels with pixel i in center, the linear function

$$I^l(j) = p_i I^h(j) + q_i, \quad j \in w_i, \tag{1}$$

provides a simple yet complete representation satisfying the local monotonic constraint. The coefficients p_i and

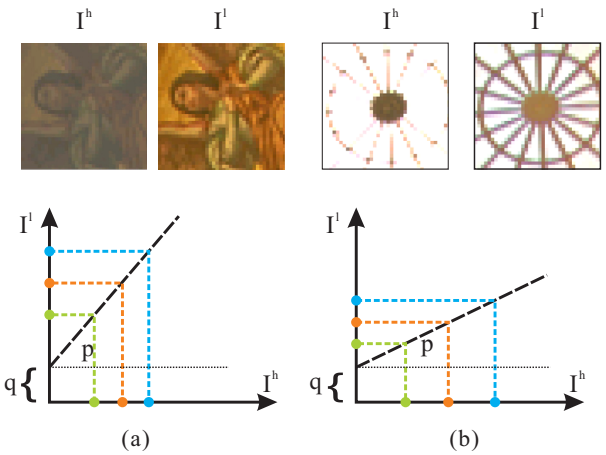

Fig. 2. Illustration of the local window operator. (a) and (b) show two configurations that I^h undergoes linear mappings (represented as the slanted dashed lines) with different coefficients p and q to produce I^l. q controls the base radiance level and p manipulates the local contrast in the window. Setting large p makes the local details in I^l be enhanced, as shown in (a), whereas a small p suppresses local high contrast, as shown in (b).

q_i, within the local window, control the mapping in two ways. The value of q determines the base radiance level while p, representing the slope of the linear function. the terms q and p directly control the local contrast as shown in Figure 2. If $p > 1$, as shown in Figure 2 (a), the local contrast is enhanced, making the result enhance details in dark regions. Figure 2 (b) shows another example where small positive p reduces image contrast and improves the visibility of structures in bright regions. Note that we do not add regularization terms, such as smoothness constraints to the overall equations. This is because p_i's and q_i's are computed in overlapping windows that contain multiple pixels. In this case, a smoothness-like constraint across pixels is naturally enforced in flat regions of an HDR image, while in regions with strong structures, such as edges, contrast is reasonably maintained.

Combining all local linear equations defined on individual windows, we can reconstruct an image by minimizing

$$\sum_i \sum_{j \in w_i} (I^l(j) - p_i I^h(j) - q_i)^2, \tag{2}$$

where i sums over all pixels in the HDR image. However, directly minimizing (2) cannot compress the high dynamic range because a trivial solution exist. For example, $p_i = 1$ and $q_i = 0$ for all i results in $I^l = I^h$ which is one solution that produces zero error in minimizing (2). As a result, additional constraints are needed. Note that p_i in (1) is the parameter directly controlling the change of local contrast. We propose guiding its value in each window to reduce the global contrast while maintaining the local visual information. We express the

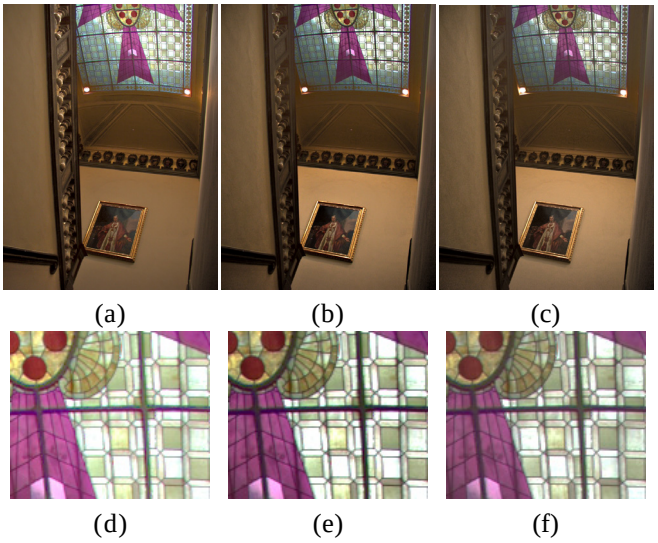

Fig. 3. Tone mapping results with window sizes (a) 3×3, (b) 7×7, and (c) 15×15. (d)-(f) Close-ups of (a)-(c) respectively.

final objective function to be minimized as

$$f = \sum_i \left(\sum_{j \in w_i} \left(I^l(j) - p_i I^h(j) - q_i \right)^2 + \varepsilon c_i^{-2} (p_i - c_i)^2 \right), \quad (3)$$

where c_i is a pre-set positive value to guide the modification of local contrast. The collective c_i in the image space form a *guidance map*. By appropriately setting the values in this map, we can suppress strong local contrasts and elevate weak ones. A detailed description of the guidance map construction is given in Section 4. The term $c_i^{-2}(p_i - c_i)^2$ in (3) is the squared relative error from the guidance map and c_i^{-2} is used to normalize the cost introduced by the difference between p_i and c_i. The term ε is a weight to balance the two terms in (3). We set its value to 0.1 in all our experiments.

The benefit of introducing the guidance map c is twofold. First, although the value of c_i influences local contrast, the configuration of c_i does not require high accuracy compared to direct modification of the radiance values in I^h. This is because in our optimization framework, ε is only a small weight, making the guidance c_i act as a soft constraint. The linear mapping term $\sum_{j \in w_i}(I^l(j) - p_i I^h(j) - q_i)^2$ also constrains modification of radiance at each pixel to be similar to the change on the neighboring pixels. This helps preserving image structure. Second, by modifying the guidance map c, our system can readily be applied to other tone management applications, such as ordinary image enhancement and HDR image synthesis. Examples are shown in Section 5.

3.1 Optimization and Implementation

Directly minimizing f in (3) is not trivial given the large set of unknowns. Methods such as gradient decent cannot be used to the global optimum because I^l, p_i and q_i are highly coupled and the energy function is not convex. However, as each pair of the linear coefficients $[p_i, q_i]$ is only defined in a single window, minimizing (3) can be expressed as

$$\arg\min_{p,q,I^l} f = \arg\min_{I^l} \sum_i \arg\min_{p_i,q_i} f_i, \quad \text{where}$$

$$f_i = \left(\sum_{j \in w_i} \left(I^l(j) - p_i I^h(j) - q_i \right)^2 + \varepsilon c_i^{-2} (p_i - c_i)^2 \right). \quad (4)$$

Using the above expression, we first compute (p_i^*, q_i^*), i.e. the optimal solution of (p_i, q_i), by setting the partial derivatives of function f_i with respect to p_i and q_i to zero and then computing the optimal $\hat{I}^l$ by solving a linear system. The computation process is described in the Appendix. We discuss in Section 4 the configuration of the guidance map c for naturally compressing the high dynamic range.

The local window size about each pixel can be adjusted in our system. In Figure 3, we show tone mapping results computed by setting window sizes from 3×3 to 15×15. For all examples shown in this paper, we found that window size 3×3 is suitable in terms of maintaining edge sharpness and computational efficiency. However, other sizes can also be used.

The above operations process the image's luminance channel. After obtaining the tone mapped radiance map $\hat{I}^l$, the RGB channels are reconstructed using the method of Schlick [23]:

$$I_k^l(i) = (I_k^h(i)/I^h(i))^s \times \hat{I}^l(i), \quad k \in \{r, g, b\} \quad (5)$$

where I_k^l is one of the RGB color channels in the image result and I_k^h is one of the color channels in the input HDR image. The term s represents the saturation factor. Larger s produces a more saturated result. The underlying idea of introducing (5) is to preserve the ratios between the luminance and color channels so that the hue of the range compressed image can be similar to that of the input HDR image. In our experiments, $s \in [0.4, 0.6]$ produces chromatically natural image results. The skeleton of our algorithm is given in Table 1.

1.	**Input**: An HDR image with radiance map I^h.
2.	**Main Steps**:
	2.1 Generate the guidance map c according to (6) in Section 4.
	2.2 Construct matrix S and B according to (18) in the Appendix.
	2.3 Compute $\hat{I}^l$ by solving the linear system defined in (17) in the Appendix.
	2.3 Restore the RGB channels I_k^l in the tone mapped result by (5).
3.	**Output**: An ordinary image with color channels I_k^l.

TABLE 1
Skeleton of our tone mapping algorithm.

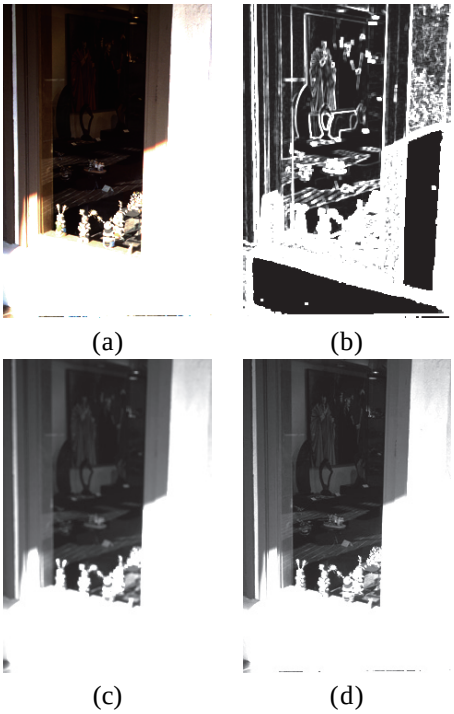

Fig. 4. "Window" example. (a) The input HDR image (image courtesy of Shree Nayar). (b) The truncated variance map of I^h on all local windows w. (c) The truncated map of mean values of I^h. (d) The truncated radiance map I^h.

4 Guidance Map Configuration in HDR Compression

In the linear optimization framework introduced in Section 3, the definition of the guidance map c principally determines the quality of HDR compression. In this section, we describe how to obtain a suitable guidance map c.

Recall that the value p_i controls the compression ratio of the dynamic range. To preserve the visual information in the tone-mapped image, we reduce the value of p_i in regions where the local contrast is large, and increase it when the local contrast is small. A measure of local contrast in each window w_i is the standard deviation σ_i of I^h. However, setting c_i inversely proportional to σ_i cannot produce a satisfying result. An example is illustrated in Figure 4 where (a) shows the input HDR image and (b) shows the variance map of I^h. The variance map is overly sensitive to the textures, edges, and even the noise in the HDR image. The HDR compression result illustrated in Figure 5 (a) is produced by setting $c_i = (\sigma_i^{\beta_2} + \kappa)^{-1}$, where $\beta_2 = 0.75$ to attenuate the variance, and κ is a small constant value. Although the high dynamic range of the original image in Figure 4(a) is reduced in the result shown in Figure 5(a), there are noticeable blemishes in the result especially in the highlighted region. These artifacts are caused by the susceptibility of the variance to the local structures.

To improve the visual quality of the result, we compute σ_i on the Gaussian filtered images to reduce noise.

Fig. 5. Illustration of the guidance map configuration. (a) The tone mapping result when c_i is set inversely proportional to the local standard deviation of I^h in each window. There are visible artifacts on the wall. (b) Magnified guidance map c. The noise is amplified. (c) The tone mapping result when c_i is configured according to (6). (d) Magnified guidance map. Note that the noise is suppressed.

Two other visual factors the local mean μ_i and the image radiance $I^h(i)$, are incorporated into the guidance map with the following considerations. First, μ_i and $I^h(i)$ represent the image radiance information. Their maps globally reflect image structures. By taking μ_i and $I^h(i)$ into the guidance formation, the over-exaggeration of structures using only local contrast can be prevented and the tonal value adjustment depends more on the input radiance in a global manner. Second, we observed that the contrast of the radiance within a local window depends largely on the absolute variance values. For instance, in Figure 4(a), the variance of the radiance inside the dark window is as low as 0.1 whereas the radiance variance in the bright windowsill is approximately 10^4. These observations indicate that incorporating μ_i and $I^h(i)$ into the guidance map construction helps suppress contrast in bright regions.

The maps of μ_i and $I^h(i)$ are illustrated in Figures 4(c) and 4(d) which emphasize the salient radiance change between the bright and dark regions while not making it highly sensitive to the isolated noise. We define c_i as

$$c_i = (\mu_i^{\beta_1} \sigma_i^{\beta_2} I^h(i)^{\beta_3} + \kappa)^{-1}, \tag{6}$$

where κ is a small weight set to 0.05 in all our experiments to prevent c_i from being divided by zero. Normally $\beta_1 \in [0.4 - 0.9]$, $\beta_2 \in [0.1 - 0.4]$, and β_3 is fixed to 0.1. We show an HDR compression result in Figure 5(c) using the guidance map constructed using (6). Comparing the magnified guidance maps shown in Figures 5(b) and 5(d), it is apparent that (d) contains much less visual artifacts.

Figure 6 shows the terms we introduced to construct the guidance map c. Figure 6(a) shows an input HDR image. The sky is bright and the hill is relatively dark. Figures 6(b) and 6(c) show the image brightness and the mean radiance in all 3×3 windows. Figure 6 (d) shows our measure of local contrast by the standard deviation

(a) (b) (c) (d) (e) (f)

Fig. 6. Illustration of the guidance map configuration. (a) An input HDR image. (b) Original radiance map $I^h(i)$. (c) Map of mean radiance μ_i. (d) Map of standard deviation σ_i. (e) The visualized guidance map c. (f) The tone mapping result using the guidance map shown in (e).

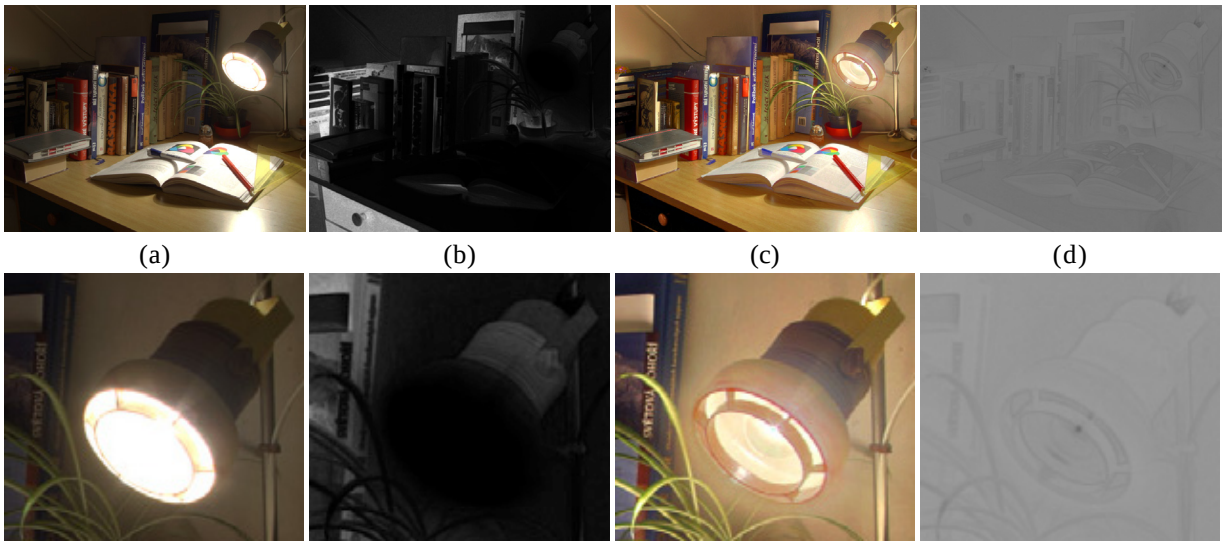

(a) (b) (c) (d)

(e) (f) (g) (h)

Fig. 7. Lamp desk. (a) An input HDR image. (b) The guidance map c generated from (a) using our method. (c) A tone-mapping result by our method. (d) The guidance map c generated from (c) using the same parameters. It is structurally flat comparing to the map shown in (b). (e)-(h) Close-ups of (a)-(d).

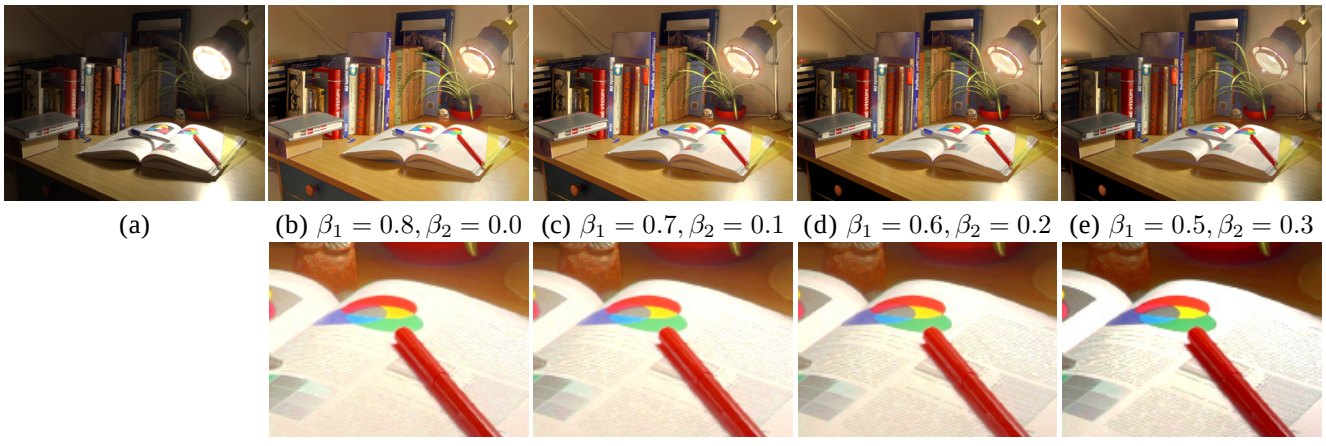

(a) (b) $\beta_1 = 0.8, \beta_2 = 0.0$ (c) $\beta_1 = 0.7, \beta_2 = 0.1$ (d) $\beta_1 = 0.6, \beta_2 = 0.2$ (e) $\beta_1 = 0.5, \beta_2 = 0.3$

(f) (g) (h) (i)

Fig. 8. HDR compression with different parameter settings. (a) shows the original HDR image, displayed with linear scaling. (b)-(e) The tone mapping results with different parameter settings. Close-ups are shown in (f)-(i).

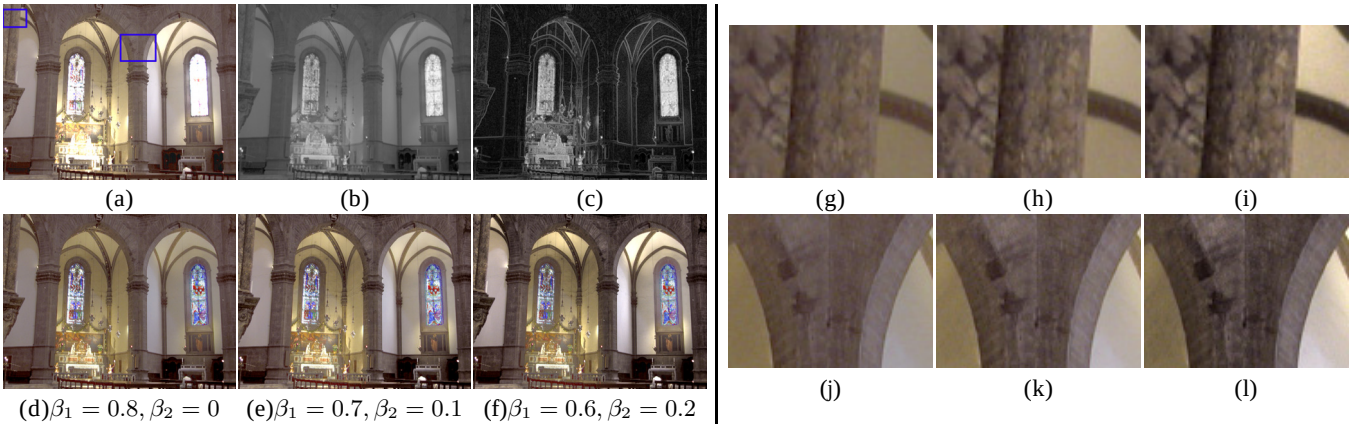

Fig. 9. HDR compression with different settings of β_1 and β_2. (a) The input HDR image. (b) Visualization of the map $log_2(\mu + 1)$. (c) Visualization of the map $log_2(\sigma + 1)$. (d)-(f) The tone mapping results with different parameter settings. We magnify two regions and compare them in (g)-(l). Local contrast is enhanced more significantly using larger β_2.

Fig. 10. HDR compression with different β_1's. (a) shows the HDR images under low exposures. (b) shows the HDR images under high exposures. (c)-(f) show our HDR compression results. In all these results, we fix $\beta_2 = 0.1$. Since $\beta_1 + \beta_2$ controls the overall compression ratio, larger $\beta_1 + \beta_2$ makes the result exhibit more details in both bright and dark regions.

of radiance σ_i (images are scaled to aid visualization). This emphasizes strong gradients or edges. The term β_2 can be used to control the compression ratio on strong edges, which in turn makes it possible to vacate more space for revealing fine local details. We show our tone mapping result in Figure 6(f), computed using the guidance map shown in Figure 6(e).

In order to preserve the details in both bright and dark regions, our algorithm balances local contrast and radiance values in the entire image. Intuitively, the guidance map constructed from a medium to low dynamic range image should be flatter in structure than that from an HDR image. To validate this, we show one example in Figure 7. The guidance map of an input HDR image (a) is shown in (b). For comparison, the guidance map of the HDR compressed image (c) is shown in (d) constructed using the same parameters. The guidance maps are linearly scaled for illustration. It can be observed that the guidance values in (d) have much smaller variations.

4.1 Parameter Settings

The parameters β_1 and β_2 can be tuned to produce different tone mapping results. We assign the values based on two principles. First, the sum of the three β's influences global dynamic range compression. Larger value makes the result visually flatter. Second, increasing β_2 enhances compression on strong edges, thus leaving more space for less salient structures.

It is notable that, in our algorithm, small modifications to β_1 and β_2 do not largely affect the result. The default values $\beta_1 = 0.6$ and $\beta_2 = 0.2$ are already capable of producing visually satisfactory results for most HDR images we have tested. To illustrate the effect of different parameter settings, we show an example in Figure 8. Image (a) shows the original HDR image. Our HDR compression results are shown in (b)-(e) using different parameter settings. In all these images, the structures on the lamp and the desk corner are augmented. Close-ups show that the text on the book is better enhanced with a larger β_2.

Figure 9 shows another example. Image (a) shows an input HDR image. The maps of μ and σ are shown in (b) and (c). The HDR compression results using different parameters are shown from (d) to (f). In all these images, details are preserved. We show the magnified regions in (g)-(l) extracted from (d)-(f). The local contrast is better preserved with larger β_2.

Figure 10 shows two examples where β_1 is set differently. The input HDR images under certain exposures are shown in (a) and (b). We fix $\beta_2 = 0.1$ and only modify β_1. Images (c)-(f) respectively show our HDR compression results with the increased sum of all β's. It can be noticed that the original high dynamic range is compressed with gradually increased ratio, and more details are maintained in both bright and dark regions using larger β_1.

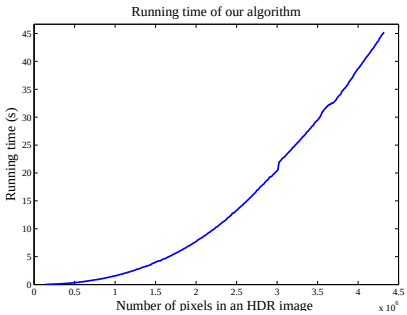

Fig. 11. Plot of running time of our tone mapping algorithm with respect to different image resolutions.

4.2 Running Time

Our algorithm is implemented using Matlab on a desktop PC with an Intel Core2Duo 2.4GHz CPU. The running time to process different images is closely related to the image resolution and is plotted in Figure 11. Taking Figure 12 as an example, the results can be obtained within 2 seconds given the image containing 512×768 pixels and with window size 3×3. We have found using larger window size for w needs more computation due to solving larger linear systems. To produce the results shown in Figure 3(a-c), our method spends 3, 25, and 150 seconds respectively in computation.

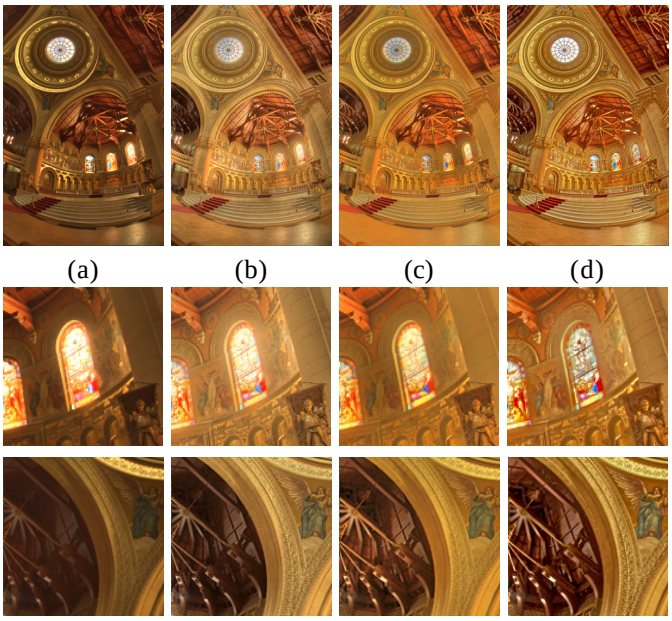

Fig. 12. Memorial Church. (a) Tone mapping result of Durand and Dorsey [7]. (b) Tone mapping result of Fattal *et al.* [9]. (c) Result by the multiscale method using one aggregated gain map [16]. (d) Our result with parameters $\beta_1 = 0.7, \beta_2 = 0.2, \beta_3 = 0.1$. (e)-(h) Magnified regions from (a)-(d) respectively. HDR image courtesy of Paul Debevec.

Fig. 13. Chairs. (a) Our tone mapping result with parameters $\beta_1 = 0.6$, $\beta_2 = 0.2$, and $\beta_3 = 0.1$. (b) The tone mapping result published in the project web page of [9]. HDR image courtesy of Shree Nayar.

4.3 More Results and Comparison

In this section, we show more HDR compression results and compare them with other state-of-the-art techniques.

In Figure 12, the tone mapping results of the HDR image "memorial church" are shown. The images in (a), (b), and (c) are published in [7], [9], and [16] respectively. Our result is illustrated in (d) with parameters $\beta_1 = 0.7, \beta_2 = 0.2, \beta_3 = 0.1$. The radiance of the dark regions, for instance the upper left corner of image, is elevated. The brightness of the stained glass window and the clerestory is reduced, revealing clear structural details. The textures and paintings on the wall and ceiling are also preserved. The magnified local regions are shown from (e) to (h).

HDR compression results of the "chairs" example

Fig. 14. Street. HDR images ©Industrial Light & Magic. The top row shows the input HDR image under different exposures. The bottom row shows our HDR compressed image reuslt and its close-ups, with parameters $\beta_1 = 0.6$, $\beta_2 = 0.2$, and $\beta_3 = 0.1$. The radiance of the sun is largely reduced.

Fig. 15. More high dynamic range compression results by our method. The parameters that produce these results are identical: $\beta_1 = 0.5$, $\beta_2 = 0.2$, and $\beta_3 = 0.1$.

by our method and the gradient-based method [9] are shown in Figures 13(a) and 13(b) respectively. More results using our optimization method are shown in Figures 14 and 15. The dynamic range is compressed from about $10^5 : 1$ to $255 : 1$. All structures, especially those originally buried in shadow and highlights, are naturally enhanced. In Figure 16, we show a comparison with the result of Farbman et al. [8].

5 Applications

5.1 Ordinary image enhancement

Our method can be extended to perform automatic enhancement of ordinary LDR images in order to improve the visibility of dark and heavily saturated regions containing structural information. The configuration of c_i, in this case, is similar to that introduced in Section 4. Since the ordinary image has much lower contrast, the values of β_1, β_2 and β_3 are set smaller. In our experiments, the default values $\beta_1 = 0.4$, $\beta_1 = 0.2$, and $\beta_3 = 0.05$ work well for most examples.

Two examples are shown in Figure 17 using the default

(a) (b)

Fig. 16. Comparison with the result of Farbman et al. [8]. (a) The tone mapped image shown in [8]. (b) Our tone mapping result.

parameter setting. In the input image (a), the mountain and its reflection in water are hardly seen. After our image enhancement, the trees and the green patterns on the mountain together with the distorted reflection are visible in (b). Images in (c) and (d) show another example. The lichen on the tree in the original image is almost unidentifiable while our result clearly enhances its details.

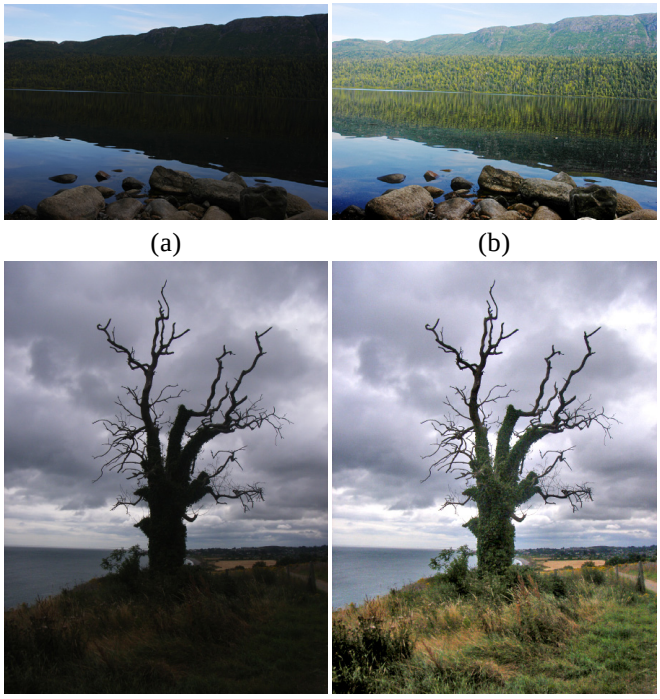

(a) (b)

(c) (d)

Fig. 17. Ordinary image enhancement. (a) and (c) The original images. (b) and (d) The automatically enhanced images showing more balanced local details and global luminance.

5.2 HDR image synthesis

In this section, we present a method for synthesizing an HDR image from a single LDR image. In our optimization framework, this process can be regarded as spatially variant dynamic range expansion. Note that in our HDR compression model, we minimize the following least square energy according to the local constraint in each window i

$$f_i = \sum_{j \in w_i} \left(I^l(j) - p_i I^h(j) - q_i \right)^2 + \varepsilon c_i^{-2} (p_i - c_i)^2. \quad (7)$$

Similarly, in the LDR expansion, we take I^l as input and compute I^h by simulating the global contrast expansion using the same model. We rewrite (7) as

$$p_i^2 \left(\sum_{j \in w_i} \left(I^h(j) - \frac{1}{p_i} I^l(j) + \frac{q_i}{p_i} \right)^2 + \varepsilon c_i^{-2} (1 - \frac{c_i}{p_i})^2 \right) \quad (8)$$

by taking p_i^2 out of the outermost parenthesis. Note that there does not exist a closed-form solution in minimizing (8) because p_i and $I^h(j)$ are both unknowns and cannot be separated in the proposed two-stage optimization. For computation simplicity, we approximate the weight p_i^2 in (8) by c_i^2. As a result, the HDR synthesis can be achieved by minimizing the energy

$$\begin{aligned} E' &= \sum_i c_i^2 \left(\sum_{j \in w_i} \left(I^h(j) - \frac{1}{p_i} I^l(j) + \frac{q_i}{p_i} \right)^2 + \varepsilon c_i^{-2} (1 - \frac{c_i}{p_i})^2 \right) \\ &= \sum_i c_i^2 \left(\sum_{j \in w_i} \left(I^h(j) - \frac{1}{p_i} I^l(j) + \frac{q_i}{p_i} \right)^2 + \varepsilon (c_i^{-1} - {p_i}^{-1})^2 \right) \end{aligned} \quad (9)$$

Denoting $p'_i = 1/p_i$, $q'_i = -q_i/p_i$, and $c'_i = 1/c_i$, (9) can be written as

$$\begin{aligned} f' \quad = \quad & \min_{p,q,I^h} \sum_i {c'}_i^{-2} \left(\sum_{j \in w_i} \left(I^h(j) - {p'}_i I^l(j) - {q'}_i \right)^2 + \right. \\ & \left. \varepsilon ({p'}_i - {c'}_i)^2 \right), \end{aligned} \quad (10)$$

in a form similar to (3) defined for HDR compression. Thus, the HDR synthesis can be dealt with within our framework by similarly employing the linear optimization.

Similar to that of HDR compression, we construct a guidance map c' incorporating the image color and structure information to appropriately constrain the LDR expansion in (10). Specifically, we use the local contrast measure σ'_i in each window w_i of I^l, the local mean μ'_i of I^l, and the image radiance $I^l(i)$ to construct the guidance map, encouraging the exaggeration of local structures in appropriate degrees. The new guidance map for (10) is expressed as

$$c'_i = ({\mu'}_i^{\beta_1} {\sigma'}_i^{\beta_2} I^l(i)^{\beta_3} + \kappa),$$

where $\kappa = 1$ to maintain or expand the image contrast. The values of β_1, β_2, and β_3 are defined similar to those in Section 4.1. In our experiments, β_3 is fixed to 0.1, $\beta_1 \in [0.4 - 0.9]$ and $\beta_2 \in [0.1 - 0.4]$.

Equation (10) can be optimized by the algorithm described in the Appendix. Since (10) is slightly different from (3), there exist variable differences on the expansion of Δ_i and S introduced in (14) and (18). Specifically, in

(a) Input (b) $\beta_1 = 0.2, \beta_2 = 0.1$ (c) $\beta_1 = 0.3, \beta_2 = 0.1$ (d) $\beta_1 = 0.4, \beta_2 = 0.2$ (e) $\beta_1 = 0.5, \beta_2 = 0.2$

Fig. 18. Image enhancement with different parameter settings. We fix $\beta_3 = 0.05$ in this example. Larger parameter values enhance more structural details.

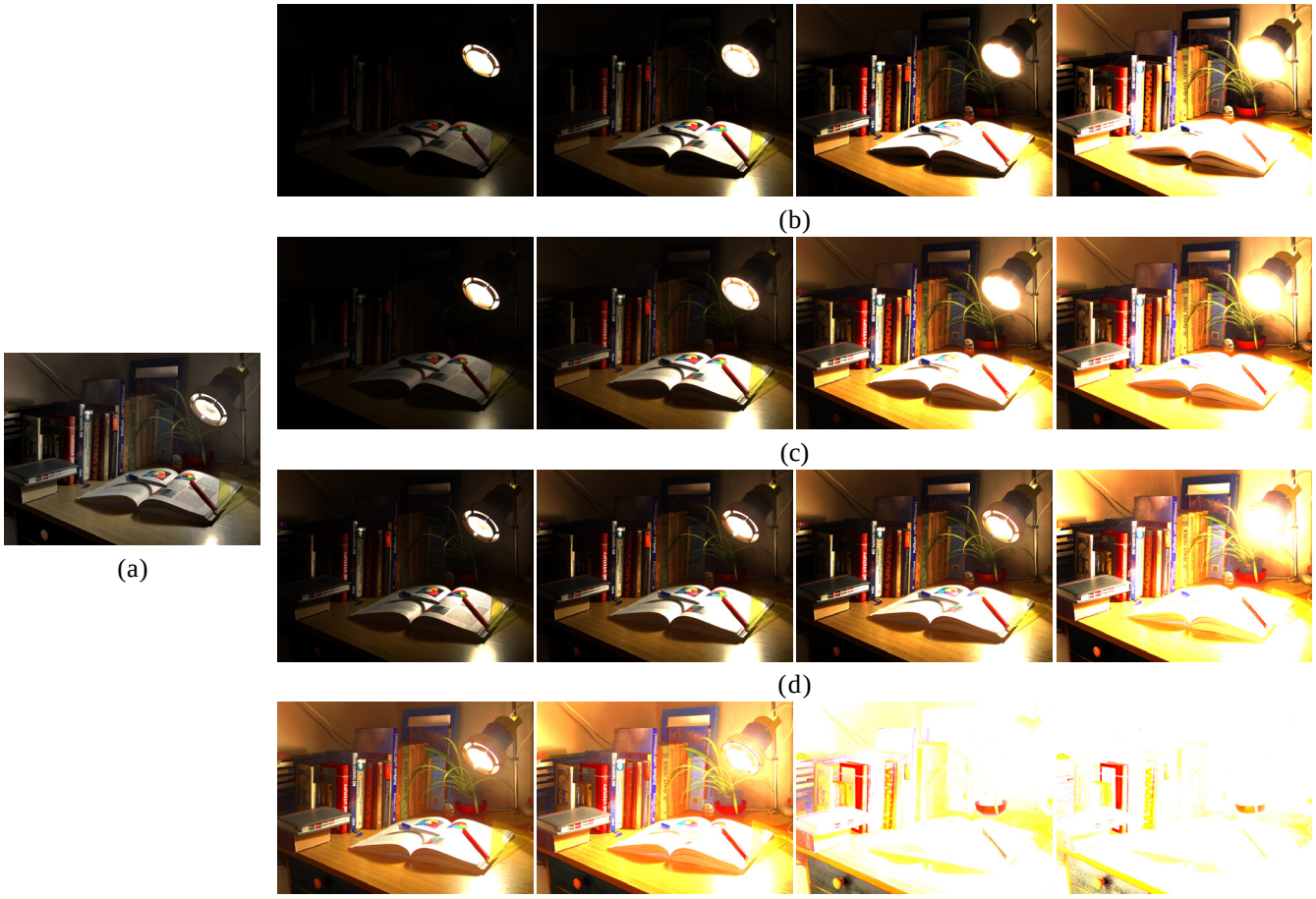

(a) (b) (c) (d) (e)

Fig. 19. HDR image synthesis. (a) The input LDR image I^l tone mapped from an HDR image I^h displayed in (b). (b) The original HDR image I^h displayed under different exposures. (c) The re-synthesized HDR image $I^{h'}$ by our algorithm (displayed under different exposures). (d) The synthesized HDR image using the LDR2HDR method [22]. (e) The synthesized HDR image using linear scaling.

the HDR synthesis, we have new Δ_i and s_{kj} defined as

$$\Delta_i = \sigma_i^2 + \left(\frac{\varepsilon}{m_i}\right),$$

$$s_{kj} = \sum_{i|\{k,j\}\subset w_i} c_i'^{-2}(\delta_{kj} - \frac{1}{m_i\Delta_i}((I^h(k) - \mu_i)(I^h(j) - \mu_i) + \Delta_i)).$$

All other variables are unchanged. The radiance expansion can be computed by solving the linear system of (17) similarly.

We denote the HDR synthesis result as $I^{h'}$ from the LDR image I^l. To evaluate the efficacy of our algorithm, we assume that the I^l is originally tone mapped from an HDR image I^h. By comparing I^h and $I^{h'}$, we are able to compute the ground truth expansion errors. In our experiments, we use Peak Signal-to-Noise Ratio (PSNR) to measure the ground truth error between the original HDR image I^h and re-synthesized image $I^{h'}$.

Two examples are shown in Figures 19 and 20. In Figure 19, the input LDR image I^l shown in (a) is compressed in dynamic range from an HDR image I^h illustrated in row (b) under different exposures. We synthesize HDR image $I^{h'}$ from I^l. The parameters are

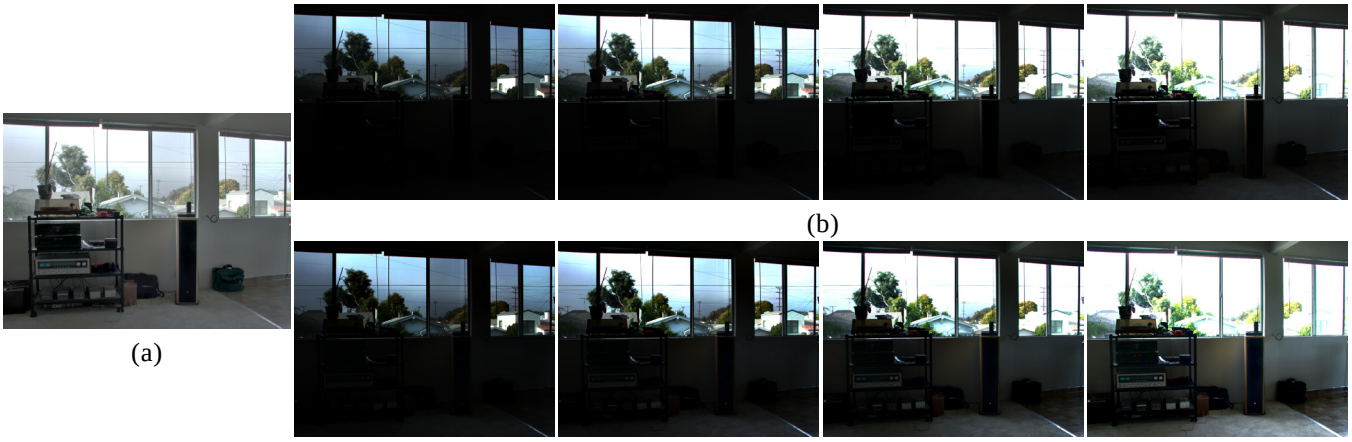

(a) (b) (c)

Fig. 20. Indoor example. (a) The input LDR image I^l compressed from an HDR image. (b) The original HDR image I^h shown under different exposures. (c) The re-synthesized HDR image $I^{h'}$ from I^l shown under different exposures.

(a) (b) (c) (d)

Fig. 21. Night view example. (a) The input LDR image. (b)-(d) Our synthesized HDR scene, shown under different exposures.

set as $\beta_1 = 0.5, \beta_2 = 0.1, \beta_3 = 0.1$ for the example shown in Figure 19, and $\beta_1 = 0.6, \beta_2 = 0.2, \beta_3 = 0.1$ for the examples shown in Figures 20 and 21. For comparison, in rows (d) and (e) of Figure 19, we show the HDR image results produced by the LDR2HDR method [22] and simple linear scaling. The PSNRs of the results in Figures 19 and 20 are 58.2873 and 57.1476 respectively , with respect to the radiance of the original HDR images.

Figure 21 shows examples of our HDR image synthesis from ordinary 8-bit LDR images. Figure 21(a) shows the input images. Images (b)-(d) are the synthesized HDR images shown under different exposures. The high-contrast illumination on the buildings and the fountains is naturally synthesized. The dynamic range is increased from 200:1 to 10^6:1 which is not possible with a single shot of a standard commodity camera. These examples describe dynamic scenes with moving persons or fountains, which are difficult to be generated using traditional methods involving multiple camera shots under different exposures.

6 Discussion and Conclusion

This paper has introduced a novel high dynamic range compression method which effectively suppresses the global contrast while preserving local image structure details. We proposed a globally non-linear method that uses overlapping window-based linear functions to reconstruct the image radiance. From a global perspective, the overlapping of the windows makes the modification of a pixel value be confined within a certain range largely depending on its neighborhood. Range compression is achieved in our method using guided linear models. Our method can also be applied to ordinary image enhancement and LDR image expanding in the same framework. The parameter adjustment is easy where a range of values are suitable for tonal adjustment.

Our method is different from multiscales approaches that require layer separation and combination steps. In

our approach, each p and q locally influence a group of pixels which in turn globally guide the optimization. We note that although our method focuses on the automatic dynamic range compression, it is not difficult to add user interactions for further interactive refinement. To modify the local radiance, the user can use stroke brushes to specify the desired values. The corresponding elements are then fixed in solving (3). The user can also modify c_i locally to adjust the level of details in the results.

APPENDIX

All the terms in the energy definition in (4) are quadratic making f_i a continuous convex function. We thus compute (p_i^*, q_i^*), the optimal solution of (p_i, q_i), by taking the partial derivatives of function f_i with respect to p_i and q_i and setting them to zeros, similar to the derivations in [15]:

$$\frac{\partial f_i}{\partial p_i}|_{p_i=p_i^*,q_i=q_i^*} = 2\varepsilon c_i^{-2}(p_i^* - c_i) + \sum_{j\in w_i} 2\left(I^l(j) - p_i^* I^h(j) - q_i^*\right)\cdot\left(-I^h(j)\right) = 0, \quad (11)$$

$$\frac{\partial f_i}{\partial q_i}|_{p_i=p_i^*,q_i=q_i^*} = \sum_{j\in w_i} -2\left(I^l(j) - p_i^* I^h(j) - q_i^*\right) = 0. \quad (12)$$

(11) and (12) are linear equations with respect to p_i and q_i, thus can be written into a matrix form

$$H_i \cdot [p_i^* \; q_i^*]^T = \eta_i, \quad (13)$$

where $H_i = \begin{bmatrix} \varepsilon c_i^{-2} + \sum_{j\in w_i} I^h(j)^2 & \sum_{j\in w_i} I^h(j) \\ \sum_{j\in w_i} I^h(j) & \sum_{j\in w_i} 1 \end{bmatrix}$ and $\eta_i = \begin{bmatrix} \varepsilon c_i^{-1} + \sum_{j\in w_i} I^h(j)\cdot I^l(j) \\ \sum_{j\in w_i} I^l(j) \end{bmatrix}$. By solving (13), we obtain

$$[p_i^* \; q_i^*]^T = H_i^{-1}\cdot\eta_i = \frac{1}{m_i\cdot\Delta_i}\begin{bmatrix} 1 & -\mu_i \\ -\mu_i & \Delta_i + \mu_i^2 \end{bmatrix}\cdot\eta_i \quad (14)$$

where

$$m_i = \sum_{j\in w_i} 1, \qquad \mu_i = \frac{1}{m_i}\sum_{j\in w_i} I^h(j),$$
$$\Delta_i = \sigma_i^2 + \left(\frac{\varepsilon c_i^{-2}}{m_i}\right).$$

After estimating p_i and q_i, we similarly compute $\hat{I}^l$, the optimal solution of (3), by taking the partial derivatives of function f with respect to $I^l(k)$ and setting them to zeros:

$$\frac{\partial f}{\partial I^l(k)}|_{I^l=\hat{I}^l} = \sum_{i|k\in w_i} 2\left(\hat{I}^l(k) - p_i^* I^h(k) - q_i^*\right) = 0. \quad (15)$$

Since f is also a continuous convex function in differentiability class C^∞ with respect to I^l, the optimal solution of I^l by solving (15) can be obtained. Combining (14) and (15), we get

$$\frac{\partial f}{\partial I^l(k)}|_{I^l=\hat{I}^l} = \sum_{i|k\in w_i}(\hat{I}^l(k) - \frac{1}{m_i\Delta_i}(\varepsilon c_i^{-1} I^h(k) + I^h(k) \sum_{j\in w_i} I^h(j)\hat{I}^l(j) - \mu_i I^h(k)\sum_{j\in w_i}\hat{I}^l(j) - \mu_i\varepsilon c_i^{-1} - \mu_i\sum_{j\in w_i} I^h(j)\hat{I}^l(j) + (\Delta_i + \mu_i^2)\sum_{j\in w_i}\hat{I}^l(j))), = 0. \quad (16)$$

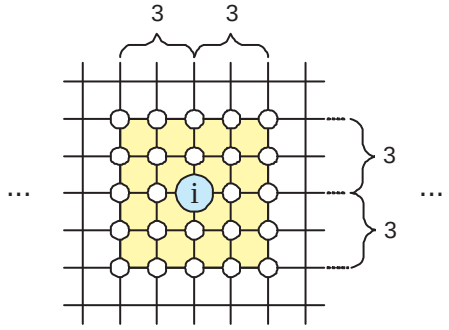

Fig. 22. Illustration of the region containing pixel i. All windows w with size 3×3 and containing i must be within the yellow region. There are at most 24 pixels in relation to i by local windows w. Since there are N pixels in an image, the total number of the non-zero elements in matrix S will be less than $25\times N$.

It can be observed that (16) is a linear combination of $\hat{I}^l$'s. We can rewrite it in a form of a large linear system

$$S\cdot\hat{I}^l = B, \quad (17)$$

where

$$s_{kj} = \frac{\partial^2 f}{\partial I^l(k)\partial\hat{I}^l(j)} = \sum_{i|\{k,j\}\subset w_i}(\delta_{kj} - \frac{1}{m_i\Delta_i}((I^h(k)-\mu_i)(I^h(j)-\mu_i) + \Delta_i)),$$
$$b_k = \sum_{i|k\in w_i}\frac{\varepsilon}{m_i\Delta_i c_i}\left(I^h(k) - \mu_i\right), \quad (18)$$

where δ_{kj} is the Kronecker delta. The optimal solution of (3) can be obtained by solving a linear system (17).

The matrix S in (17) is symmetric and sparse. In each row i of S, the number of nonzero elements is up to a defined region size according to (17). Given an input image containing N pixels and the size of the window w_i set to $k\times k$, S has less than $(2k-1)^2\times N$ non-zero elements (a $k=3$ example is shown in Figure 22). Mathematically, the minimum possible window size is 2×2, as there are three unknowns in each local window and at least three linear constraints are needed to make the problem well-posed.

If the image has moderate resolution, it is still possible to directly apply the symmetric LQ or generalized minimum residual methods to solving the linear system (17) in Matlab. However, to process an image with resolution higher than 1000×1000, the above methods will take several minutes to converge. To accelerate, a multigrid method [10], same as the one used in [15], is employed which produces a satisfactory $\hat{I}^l$ in only seconds in all our experiments.

ACKNOWLEDGMENTS

The authors would like to thank the associate editor and all reviewers for their constructive comments to improve the manuscript. This work was supported by a grant from the Research Grants Council of the Hong

Kong Special Administrative Region, China (Project No. 412708), a grant from SHIAE (No. 8115016), and an AcRF Tier 1 Singapore grant (Project No. R-252-000-333-133).

REFERENCES

[1] A. O. Akyüz, R. Fleming, B. E. Riecke, E. Reinhard, and H. H. Bülthoff. Do HDR displays support LDR content? a psychophysical evaluation. In *SIGGRAPH*, page 38, 2007.
[2] M. Ashikhmin. A tone mapping algorithm for high contrast images. In *Proceedings of the 13th Eurographics workshop on Rendering*, pages 145–156, 2002.
[3] F. Banterle, P. Ledda, K. Debattista, and A. Chalmers. Inverse tone mapping. In *GRAPHITE*, pages 349–356, 2006.
[4] K. Chiu, M. Herf, P. Shirley, S. Swamy, C. Wang, and K. Zimmerman. Spatially nonuniform scaling functions for hight contrast images. In *Graphics Interface*, pages 245–253, 1993.
[5] K. Devlin. A review of tone reproduction techniques. Technical Report CSTR-02-005, 2002.
[6] J. Duan, G. Qiu, and M. Chen. Comprehensive fast tone mapping for high dynamic range image visualization. In *Pacific Graphics*, 2005.
[7] F. Durand and J. Dorsey. Fast bilateral filtering for the display of high-dynamic-range images. In *SIGGRAPH*, pages 257–266, 2002.
[8] Z. Farbman, R. Fattal, D. Lischinski, and R. Szeliski. Edge-preserving decompositions for multi-scale tone and detail manipulation. In *SIGGRAPH*, 2008.
[9] R. Fattal, D. Lischinski, and M. Werman. Gradient domain high dynamic range compression. In *SIGGRAPH*, pages 249–256, 2002.
[10] W. W. Hager, S.-J. Huang, P. M. Pardalos, and O. A. Prokopyev. *Multiscale Optimization Methods and Applications (Nonconvex Optimization and Its Applications)*. Springer, 2005.
[11] B. K. P. Horn. Determining lightness from an image. *Computer Graphics and Image Processing*, 3:277–299, 1974.
[12] D. J. Jobson, Z. Rahman, and G. A. Woodell. A multiscale retinex for bridging the gap between color images and the human observation of scenes. *IEEE Transaction of Image Processing*, 6(7):965–976, 1997.
[13] G. Krawczyk, K. Myszkowski, and H.-P. Seidel. Computational model of lightness perception in high dynamic range imaging. In *IS&T/SPIE's Human Vision and Electronic Imaging*, 2006.
[14] G. W. Larson, H. Rushmeier, and C. Piatko. A visibility matching tone reproduction operator for high dynamic range scenes. *IEEE Transactions on Visualization and Computer Graphics*, 3(4):291–306, 1997.
[15] A. Levin, D. Lischinski, and Y. Weiss. A closed form solution to natural image matting. In *CVPR*, 2006.
[16] Y. Li, L. Sharan, and E. H. Adelson. Compressing and companding high dynamic range images with subband architectures. In *SIGGRAPH*, pages 836–844, 2005.
[17] D. Lischinski, Z. Farbman, M. Uyttendaele, and R. Szeliski. Interactive local adjustment of tonal values. In *SIGGRAPH*, pages 646–653, 2006.
[18] L. Meylan, S. Daly, and S. Süsstrunk. The reproduction of specular highlights on high dynamic range displays. In *Color Imaging Conference*, 2006.
[19] S. N. Pattanaik, J. A. Ferwerda, M. D. Fairchild, and D. P. Greenberg. A multiscale model of adaptation and spatial vision for realistic image display. In *SIGGRAPH*, pages 287–298, 1998.
[20] E. Reinhard, M. Stark, P. Shirley, and J. Ferwerda. Photographic tone reproduction for digital images. *SIGGRAPH*, 21(3):267–276, 2002.
[21] E. Reinhard, G. Ward, S. Pattanaik, and P. Debevec. *High Dynamic Range Imaging*. Morgan Kaufman, 2005.
[22] A. G. Rempel, M. Trentacoste, H. Seetzen, H. D. Young, W. Heidrich, L. Whitehead, and G. Ward. Ldr2hdr: on-the-fly reverse tone mapping of legacy video and photographs. In *SIGGRAPH*, page 39, 2007.
[23] C. Schlick. A customizable reflectance model for everyday rendering. In *Fourth Eurographics Workshop on Rendering*, pages 73–83, 1993.
[24] T. G. Stockham. Image processing in the context of a visual model. *Proceedings of the IEEE*, 60(7):828–842, 1972.
[25] J. Tumblin. *Three methods of detail-preserving contrast reduction for displayed images*. PhD thesis, Georgia Institute of Technology, 1999.
[26] J. Tumblin and G. Turk. LCIS: a boundary hierarchy for detail-preserving contrast reduction. In *SIGGRAPH*, pages 83–90, 1999.

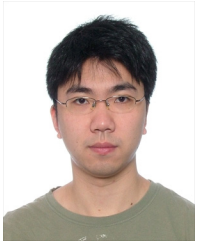

Qi Shan received the joint Bachelor degree from Fudan University in China and University College Dublin in Ireland in 2006 and the MPhil degree in computer science from the Chinese University of Hong Kong in 2008. Currently, he is a PhD student in the Department of Computer Science and Engineering in the University of Washington, Seattle. His research interests include computer graphics and vision. He is an IEEE student member.

Jiaya Jia received the PhD degree in computer science from the Hong Kong University of Science and Technology in 2004. He joined the Department of Computer Science and Engineering, Chinese University of Hong Kong, in September 2004, where he is currently an assistant professor. His research interests include vision geometry, image/video editing and enhancement, and motion deblurring. He has served on the program committees of ICCV, CVPR, ECCV, and ACCV. He served as co-chair of the interactive computer vision workshop 2007 (in conjunction with ICCV07). He is a member of IEEE.

Michael S. Brown obtained his BS and PhD in Computer Science from the University of Kentucky in 1995 and 2001 respectively. He is currently the Sung Kah Kay Assistant Professor in the School of Computing at the National University of Singapore. His research interests include Computer Vision, Image Processing and Computer Graphics. He served as the general co-chair for the 5th ACM/IEEE Projector-Camera-Systems (PROCAMS08) workshop co-located with SIGGRAPH08 and is an organizer for the eHeritage09 Workshop co-located with ICCV09. He was an Area Chair for CVPR'09. He is a member of IEEE.